Archives of Acoustics Online First June 22, 2025 https://doi.org/10.24425/aoa.2025.154815

Research Paper

Experimental and Computational Analysis on the Acoustic Performance of Side Outlet Muffler with Semi-Circular Baffles

Sandeep Kumar VISHWAKARMA, Suryappa Jayappa PAWAR*

Department of Applied Mechanics, Motilal Nehru National Institute of Technology Allahabad Prayagraj, India

*Corresponding Author e-mail: sjpawar@mnnit.ac.in

Received December 7, 2023; revised March 4, 2025; accepted June 10, 2025; published online July 22, 2025.

In this study, the impacts of the inclusion of two semi-circular baffles and their orientations on the acoustic performance of the side outlet muffler have been investigated. The side outlet muffler has a circular simple expansion chamber with an axial inlet and a side outlet and two semi-circular baffles that have been placed inside the expansion chamber at different orientations. The axis of the outlet is at the right angle to the axis of the inlet. The acoustical investigation of the side outlet muffler with two semi-circular baffles is done using the plane wave analysis, the finite element method (FEM), and the two-load technique. Based on the orientations of the two semi-circular baffles, three different models of side outlet muffler with semi-circular baffles have been investigated. The plane wave analysis, FEM, and two-load method are applied to all models and it is found that analytical, computational, and experimental transmission loss (TL) are in good agreement. The analytical modelling successfully predicts the presence of semi-circular baffles in the form of peaks and troughs in the TL of side outlet muffler with semi-circular baffles before the cut-off frequency and thus proves its effectiveness. Among all the models, model_2 gives 42 % higher TL than model_1 and model_3 shows 16.20 % higher TL than model_2. Hence, model_3 proves to be the best design for the side outlet muffler with semi-circular baffles in the attenuation of noise. The model_3 is effective for 1030 Hz–1480 Hz, 1500 Hz–1570 Hz, and 1640 Hz–2400 Hz frequency sound waves. The TL curve, sound pressure contours for model_3, and the band power variation in the 1/3 octave band for all the models have also been presented.

Keywords: band power; finite element method; semi-circular baffles; side outlet muffler; sound pressure level; transmission loss; two-load method.

1. Introduction

Reactive mufflers (Reddy *et al.*, 2017) work by decreasing exhaust noise by adjusting the volume based on sound reflections (Mundhe, Deore, 2015). The plane wave effect (Davis *et al.*, 1954) has been used to analyze mufflers. Munjal (1975) suggested an enhanced 4-pole transfer matrix based on fluid dynamics. Some researchers (Igarashi, 1958; Jeong *et al.*, 2015; Xiang *et al.*, 2016) also used the 4-pole transfer matrix to forecast the acoustic performance of mufflers. Sullivan and Crocker (1978) established linked equations for the inner and outer pipes of a perforated muffler (Sullivan, 1979). The solution for the linked equations was reported by Jayaraman and Yam (1981). As the solutions were based on the one-dimensional wave theory, without capturing the effect of higher-order modes of the wave. Ih and Lee (1985; 1987) investigated a muffler with an expansion chamber at a higher-order mode to solve the shortcomings of the plane wave theory. Åbom (1990) created a transfer matrix for an expanded muffler with a circular portion considering the higher-order modes. Munjal (1987) used a numerical method (analytic method) to make the calculation procedure simple, but there was a limitation in the area ratio (only integer values were allowed). When the inlet and the outlet were perpendicular to each other, the analytical method was not able to analyze that muffler. Ih (1992) proposed a numerical methodology for the evaluation of the acoustic char-

acteristics of two designs of the muffler. The mufflers with rectangular and circular cross-sections were taken into consideration. Chang and Chiu (2014) suggested a simplified artificial neural network (ANN) model in combination with the boundary element method (BEM) (Seybert, Cheng, 1987; Wang, 1999), the finite element method (FEM) (Zheng *et al.*, 2012), and the evolutionary technique to optimize the design of the rectangular-shaped mufflers. Simple baffles were also incorporated into this rectangular muffler. Yi and Lee (1986) analyzed the excitation of the higher-order modes in a circular expansion chamber with the side inlet and side outlet muffler. Munjal (1997) derived the 4-pole parameters for the side inlet and side outlet elements and compared their performance with the extended inlet and extended outlet. Kulkarni and Ingle (2018) studied the consequence of the placement of the outlet section on the transmission loss (TL) (Zhao, Li, 2022; Gorazd, 2021; Mohamad *et al.*, 2021) of the reactive muffler having two expansion chamber.

The TL is typically measured using 4-pole methods or 3-point (decomposition method), the two-load method, and the two-source method (Tao, Seybert, 2003). The popular computational softwares for evaluation of the TL of the mufflers are Actran and COMSOL Multiphysics (using FEM (Mimani, Munjal, 2012; Yu *et al.*, 2016; Narayana, Munjal, 2005)), COUSTYX (using BEM (Narayana, Munjal, 2005)), and Ricardo wave (using transfer matrix techniques (Gupta, 2016a)). The baffles are used in the expansion chamber to suppress unwanted sound by directing the exhaust gas to travel a longer distance (Das *et al.*, 2022). The usage of the baffles in the mufflers has been shown to improve the TL (Done *et al.*, 2014; Gupta, 2016b; Le Roy, 2011) by more than 50 %. Le Roy (2011) used harmonic BEM with LMS's Virtual Lab Acoustics module to explore the effect of interior baffles. Horoub (2011) investigated the multiple connected expansion chambers and documented the impact of the tapered expansion chambers. The effect of the hole pattern on the TL has also been examined by Gupta and Tiwari (2015). The flow of exhaust gases along with the sound wave through the muffler also influence the performance of the muffler. The mean flow of gases inside the muffler causes a general flattening of TL curve, where all the peaks and troughs were almost completely removed and there was a general decrease in TL (Fairbrother, Varhos, 2007; Siano *et al.*, 2010; Cheng, Wu, 1999). The other effect of the mean flow is the aerodynamic noise generated due to the turbulence of flow of the gases inside the muffler (Le Roy, 2011). The Mach number in the flow of exhaust gases of automotive engine is generally in between 0.1 and 0.3 (Munjal, 1975; Fan, Guo, 2016), and the aerodynamic noise is considered to be weak. Therefore, the aerodynamic noise may be disregarded (Ih, Lee, 1987; Mimani, Munjal, 2011). The effect of mean flow on the performance of muffler is not considered.

The previously published research (Das *et al.*, 2022; Done *et al.*, 2014; Gupta, 2016b; Le Roy, 2011) provides the motivation to use baffles in the side outlet muffler. These studies have shown that baffles can increase the TL of the muffler by a reasonable amount. The baffles are used to change the impedance and thus promoting the reflection of the sound waves (Das *et al.*, 2022). This reflection of sound wave can cause the destructive interference with the incoming sound wave and hence reduces the intensity of sound wave. Additionally, baffles also deflect the sound waves to travel longer paths and hence dissipating the acoustic energy of the sound waves (Gupta, 2016b). Based on the suppression of noise of different frequencies, the baffles can have the different shapes and the orientations inside the expansion chamber of mufflers. The reflection of sound waves depends upon the area discontinuity introduced due to the baffles (Elsayed *et al.*, 2017), orientation of the baffles, and spacing between the baffles (Das *et al.*, 2022). In this work, baffles are designed to decrease the cross-sectional area of the expansion chamber by 50 % at the area discontinuity. Since, the expansion chamber of side outlet muffler has a circular cross-section, the semi-circular shaped baffles are used in this study. Along with the area discontinuity due to the semi-circular baffles, the effect of their orientation inside the expansion chamber is also examined.

The impacts of the two semi-circular baffles and their orientation on the acoustical performance of the side outlet muffler have been investigated in this study. Based on the orientation of the semi-circular baffles, three models of the side outlet muffler with semi-circular baffles (SOMWB) have been investigated in this study. The models differ in the orientation of the two semi-circular baffles along the length of the simple expansion chamber of the side outlet muffler. The plane wave analysis, FEM, and two load method are used for the analytical modelling, computational modelling, and experimentation of all the models of the SOMWB, respectively. The analytical and computational results are compared with the experimental results and a fair agreement is found. The band power variation in the 1/3 octave band for all the cases of the SOMWB and sound pressure level (SPL) contours at the desired frequencies for the best model of the SOMWB (model_3) have also been presented.

2. Analytical modelling

The analytical modelling of a plane traveling wave uses the continuity condition and mass conservation. The pressure for a one-dimensional traveling wave is the superposition of an incident wave and a reflected wave. The pressure equation contains separate terms for the incident and reflected waves. The modelling is

done for the sound wave travelling inside the SOMWB. The SOMWB is divided into A, B, C, D, E, F, and G regions and incident and reflected waves for the different regions have been shown in Fig. 1. The distance between the two semi-circular baffles, thickness of baffles, distance of the baffles from the ends of the expansion chamber, length of baffles, distance of the right side baffle from the centre of the outlet pipe, length of the expansion chamber, and diameter of the expansion chamber are represented by d, w, s, l, and t, a_x, and a_y, respectively. The A-region is from $x = -s - w$ to $x = -s$, B-region is from $x = -s$ to $x = 0$, C-region is from $x = 0$ to $x = w$, D-region is from $x = w$ to $x = w+d$, E-region is from $x = w + d$ to $x = 2w + d$, F-region is from $x = 2w + d$ to $x = 2w + d + t$, and G-region is from $x = 2w + d + t$ to $x = 2w + d + s$. The coefficients for incident and reflected wave in different regions are given by A^+, A^-, B^+, B^-, C^+, C^-, D^+, D^-, E^+, E^-, F^+, F^-, G^+, and G^-, respectively.

The pressure fields and the velocity components in the A-region, B-region, C-region, D-region, E-region, F-region, and G-region can be written as (Lee *et al.*, 2019; Vishwakarma, Pawar, 2022):

$$P_A = A^+e^{-ik(x+s)} + A^-e^{ik(x+s+w)}, \tag{1}$$

$$u_A = \frac{A^+e^{-ik(x+s)} - A^-e^{ik(x+s+w)}}{\frac{c}{S_A}}, \tag{2}$$

$$P_B = B^+e^{-ikx} + B^-e^{ik(x+s)}, \tag{3}$$

$$u_B = \frac{B^+e^{-ikx} - B^-e^{ik(x+s)}}{\frac{c}{S_B}}, \tag{4}$$

$$P_C = C^+e^{-ikx} + C^-e^{ik(x-w)}, \tag{5}$$

$$u_C = \frac{C^+e^{-ikx} - C^-e^{ik(x-w)}}{\frac{c}{S_C}}, \tag{6}$$

$$P_D = D^+e^{-ik(x-w)} + D^-e^{ik(x-w-d)}, \tag{7}$$

$$u_D = \frac{D^+e^{-ik(x-w)} - D^-e^{ik(x-w-d)}}{\frac{c}{S_D}}, \tag{8}$$

$$P_E = E^+e^{-ik(x-w-d)} + E^-e^{ik(x-2w-d)}, \tag{9}$$

$$u_E = \frac{E^+e^{-ik(x-w-d)} - E^-e^{ik(x-2w-d)}}{\frac{c}{S_E}}, \tag{10}$$

$$P_F = F^+e^{-ik(x-2w-d)} + F^-e^{ik(x-2w-d-t)}, \tag{11}$$

$$u_F = \frac{F^+e^{-ik(x-2w-d)} - F^-e^{ik(x-2w-d-t)}}{\frac{c}{S_F}}, \tag{12}$$

$$P_G = G^+e^{-ik(x-2w-d-t)} + G^-e^{ik(x-2w-d-s)}, \tag{13}$$

$$u_G = \frac{G^+e^{-ik(x-2w-d-t)} - G^-e^{ik(x-2w-d-s)}}{\frac{c}{S_G}}. \tag{14}$$

By continuity condition in the B-region and C-region, the pressure at the points just before the discontinuity and just after the discontinuity is equal, i.e., at $x = 0$:

$$P_B = P_C, \tag{15}$$

$$B^+ + B^-e^{iks} = C^+ + C^-e^{-ikw}. \tag{16}$$

By mass conservation condition, the mass of the particle is constant across all the junctions. Since the density of the medium is taken as constant, instead of mass one can equate the volume particle velocity at the discontinuities, i.e., at $x = 0$:

$$u_B = u_C, \tag{17}$$

$$B^+ - B^-e^{iks} = \left(C^+ - C^-e^{-ikw}\right)\frac{S_C}{S_B}. \tag{18}$$

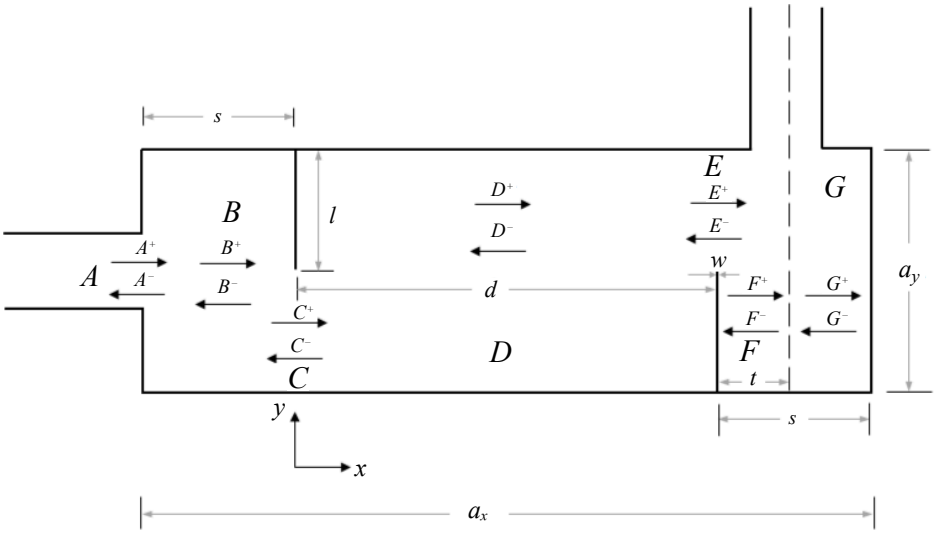

Fig. 1. Different regions of side outlet muffler with semi-circular baffles.

From Eqs. (16) and (18), one can write the relation between coefficients in the B-region and C-region as

$$\begin{bmatrix} B^+ \\ B^- \end{bmatrix} = \begin{bmatrix} 0.5\left(1+\frac{S_C}{S_B}\right) & -0.5\left(\frac{S_C}{S_B}-1\right)e^{-ikw} \\ 0.5\left(1-\frac{S_C}{S_B}\right)e^{-iks} & 0.5\left(1+\frac{S_C}{S_B}\right)e^{-ik(w+s)} \end{bmatrix} \begin{bmatrix} C^+ \\ C^- \end{bmatrix}, \tag{19}$$

$$\begin{bmatrix} B^+ \\ B^- \end{bmatrix} = [M_1] \begin{bmatrix} C^+ \\ C^- \end{bmatrix}. \tag{20}$$

Similarly, relations among the other coefficient can be written as

$$\begin{bmatrix} A^+ \\ A^- \end{bmatrix} = \begin{bmatrix} 0.5\left(1+\frac{S_B}{S_A}\right)e^{iks} & -0.5\left(\frac{S_B}{S_A}-1\right) \\ 0.5\left(1-\frac{S_B}{S_A}\right)e^{ik(s-w)} & 0.5\left(1+\frac{S_B}{S_A}\right)e^{-ikw} \end{bmatrix} \begin{bmatrix} B^+ \\ B^- \end{bmatrix}, \tag{21}$$

$$\begin{bmatrix} A^+ \\ A^- \end{bmatrix} = [M_2] \begin{bmatrix} B^+ \\ B^- \end{bmatrix}, \tag{22}$$

$$\begin{bmatrix} C^+ \\ C^- \end{bmatrix} = \begin{bmatrix} 0.5\left(1+\frac{S_D}{S_C}\right)e^{ikw} & -0.5\left(\frac{S_D}{S_C}-1\right)e^{-ik(d+w)} \\ -0.5\left(1-\frac{S_D}{S_C}\right)e^{2ikw} & 0.5\left(1+\frac{S_D}{S_C}\right)e^{-ikd} \end{bmatrix} \begin{bmatrix} D^+ \\ D^- \end{bmatrix}, \tag{23}$$

$$\begin{bmatrix} C^+ \\ C^- \end{bmatrix} = [M_3] \begin{bmatrix} D^+ \\ D^- \end{bmatrix}, \tag{24}$$

$$\begin{bmatrix} D^+ \\ D^- \end{bmatrix} = \begin{bmatrix} 0.5\left(1+\frac{S_E}{S_D}\right)e^{ikd} & -0.5\left(\frac{S_E}{S_D}-1\right)e^{-ik(w-d)} \\ 0.5\left(1-\frac{S_E}{S_D}\right) & 0.5\left(1+\frac{S_E}{S_D}\right)e^{-ikw} \end{bmatrix} \begin{bmatrix} E^+ \\ E^- \end{bmatrix}, \tag{25}$$

$$\begin{bmatrix} D^+ \\ D^- \end{bmatrix} = [M_4] \begin{bmatrix} E^+ \\ E^- \end{bmatrix}, \tag{26}$$

$$\begin{bmatrix} E^+ \\ E^- \end{bmatrix} = \begin{bmatrix} 0.5\left(1+\frac{S_F}{S_E}\right)e^{ikw} & -0.5\left(\frac{S_F}{S_E}-1\right)e^{ik(w-t)} \\ 0.5\left(1-\frac{S_F}{S_E}\right) & 0.5\left(1+\frac{S_F}{S_E}\right)e^{-ikt} \end{bmatrix} \begin{bmatrix} F^+ \\ F^- \end{bmatrix}, \tag{27}$$

$$\begin{bmatrix} E^+ \\ E^- \end{bmatrix} = [M_5] \begin{bmatrix} F^+ \\ F^- \end{bmatrix}, \tag{28}$$

$$\begin{bmatrix} F^+ \\ F^- \end{bmatrix} = \begin{bmatrix} 0.5\left(1+\frac{S_G}{S_F}\right)e^{ikt} & -0.5\left(\frac{S_G}{S_F}-1\right)e^{ik(2t-s)} \\ 0.5\left(1-\frac{S_G}{S_F}\right) & 0.5\left(1+\frac{S_G}{S_F}\right)e^{ik(t-s)} \end{bmatrix} \begin{bmatrix} G^+ \\ G^- \end{bmatrix}, \tag{29}$$

$$\begin{bmatrix} F^+ \\ F^- \end{bmatrix} = [M_6] \begin{bmatrix} G^+ \\ G^- \end{bmatrix}, \tag{30}$$

where $[M_1]$, $[M_2]$, $[M_3]$, $[M_4]$, $[M_5]$, and $[M_6]$ are the coefficient matrices among different regions. The relation between the coefficient of A-region and G-region can be obtained by the multiplication of the coefficient matrices of different regions. The relation can be written as

$$\begin{bmatrix} A^+ \\ A^- \end{bmatrix} = [M_2][M_1][M_3][M_4][M_5][M_6]\begin{bmatrix} G^+ \\ G^- \end{bmatrix}, \quad (31)$$

$$\begin{bmatrix} A^+ \\ A^- \end{bmatrix} = [GM]\begin{bmatrix} G^+ \\ G^- \end{bmatrix}. \quad (32)$$

In G-region, the velocity component at $x = 2w+d+s$ becomes zero. Therefore, u_G can be written as

$$\frac{G^+ e^{-ik(x-2w-d-t)} - G^- e^{ik(x-2w-d-s)}}{\frac{c}{S_G}} = 0, \quad (33)$$

$$G^- = G^+ e^{-ik(s-t)}. \quad (34)$$

By using the relation between G^- and G^+ in Eq. (32), one can write

$$\begin{bmatrix} A^+ \\ A^- \end{bmatrix} = [GM]\begin{bmatrix} 1 \\ e^{-ik(s-t)} \end{bmatrix} G^+. \quad (35)$$

From Eq. (35), one can easily obtain the ratio of A^+ to G^+. Therefore the TL of the SOMWB can be given by (Vishwakarma, Pawar, 2021):

$$\mathrm{TL} = 20\log_{10}\left(\frac{A^+}{G^+}\right). \quad (36)$$

3. Computational modelling

The FEA has been used for the computational modelling of SOMWB. The computational modelling of mufflers requires pressure and velocity equations (Lee *et al.*, 2019). The TL is evaluated with the help of the pressure and velocity equations. The governing equations in ANSYS (2022) are used for the acoustic modelling of muffler with assumptions such as absence of mean flow, no fluid-structure interaction, compressible and irrotational fluid medium, and an anechoic termination at the outlet.

In acoustic modelling, Navier–Stokes (NS) equations of fluid momentum and the continuity are used for the formulation of acoustic wave equations (ANSYS, 2022).

The continuity equation is

$$\frac{\partial \rho}{\partial t} = -\nabla \cdot (\rho \mathbf{v}) + Q, \quad (37)$$

where ρ, t, $\mathbf{v}$, and Q are the density, time, velocity vector in the x-, y-, and z-directions, and mass source ($\mathrm{kg/m^3t}$), respectively.

The Navier–Stokes equation is

$$\rho\frac{\mathrm{d}\mathbf{v}}{\mathrm{d}t} = -\nabla p + \nabla \cdot \overline{\overline{S}} + \rho\mathbf{b}, \quad (38)$$

where p, $\overline{\overline{S}}$, and $\mathbf{b}$ are pressure, viscous stress tensor, and body force, respectively.

The continuity and NS equations are linearized to obtain the acoustic wave equation. The resulting linearized forms are as follows:

$$\nabla \cdot \mathbf{v}_a = -\frac{1}{\rho c^2}\frac{\partial^2 p_a}{\partial t^2} + \frac{Q}{\rho}, \quad (39)$$

$$\frac{\partial \mathbf{v}_a}{\partial t} = -\frac{1}{\rho}\nabla p_a + \frac{4}{3}\frac{\mu}{\rho}\nabla\left(-\frac{1}{\rho c^2}\frac{\partial p_a}{\partial t} + \frac{Q}{\rho}\right), \quad (40)$$

where $\mathbf{v}_a$, p_a, c, and μ are the acoustic velocity, acoustic pressure, speed of sound, and dynamic viscosity of the medium, respectively.

From Eqs. (39) and (40) acoustic wave equation can be formulated as

$$\nabla \cdot \left(\frac{1}{\rho}\nabla p_a\right) - \frac{1}{\rho c^2}\frac{\partial^2 p_a}{\partial t^2} + \nabla \cdot \left[\frac{4}{3}\frac{\mu}{\rho}\nabla\left(\frac{1}{\rho c^2}\right)\frac{\partial p_a}{\partial t}\right] = -\frac{\partial}{\partial t}\left(\frac{Q}{\rho}\right) + \nabla \cdot p\left[\frac{4}{3}\frac{\mu}{\rho}\nabla\left(\frac{Q}{\rho}\right)\right]. \quad (41)$$

The SPL is given by Eq. (42), where p_{rms} and p_{ref} are the root mean square of peak pressure in harmonic analysis and reference pressure (2×10^{-5} Pa), respectively:

$$\mathrm{SPL} = 10\log_{10}\left(\frac{p_{\mathrm{rms}}^2}{p_{\mathrm{ref}}^2}\right). \quad (42)$$

The TL is given by Eq. (43), where

$$P_{in} = \frac{p_{in}^2}{\rho c} \quad \text{and} \quad P_t = \frac{p_o^2}{\rho c}$$

are the incident sound power at the inlet and the transmitted sound power at the outlet, and p_{in} and p_o are the sound pressure at the inlet and at outlet, respectively:

$$\mathrm{TL} = 10\log_{10}\left(\frac{P_{in}}{P_t}\right). \quad (43)$$

The radiation boundary condition is applied at the inlet and outlet of the muffler. The radiation boundary condition takes care of the anechoic termination. The surface velocity condition is applied at the inlet of the muffler to create the source of the disturbance in the medium. The walls of the domain and semi-circular baffles are set to the rigid wall to apply the Neumann boundary conditions. Ports are defined to calculate the TL of the muffler.

3.1. Side outlet muffler with semi-circular baffles (SOMWB)

The proposed SOMWB is the outcome of the inclusion of the semi-circular baffles and adjustments made in the position of the outlet in a simple expansion chamber (SEC) muffler (Tao, Seybert, 2003). The position of the outlet and orientation of two semi-circular baffles are shown in Figs. 2a–2c. There are three variations in the orientation of the two semi-circular baffles inside the SOM. Based on the variations, models such as model_1, model_2, and model_3 are analysed and shown in Fig. 2. The orientations of semi-circular baffles in model_1 and model_2 are the same and can be seen in X-X planes of Figs. 2a and 2b. In model_1, the first semi-circular baffle is placed on the upper half of the expansion chamber, and the second semi-circular baffle is placed on the lower half of the expansion chamber. Whereas, in model_2, the first semi-circular baffle is placed on the lower half of the expansion chamber, and the second semi-circular baffle is placed on the upper half of the expansion chamber. On the other hand, model_3 has a different orientation of semi-circular baffles and is shown in Fig. 2c. The orientation of semi-circular baffles can be seen in the X-X plane of the model_3 of SOMWB. The first semi-circular baffle is placed on the left half and second semi-circular baffle is placed on the right half of the expansion chamber. The analysis is carried out in the harmonic acoustic module. The com-

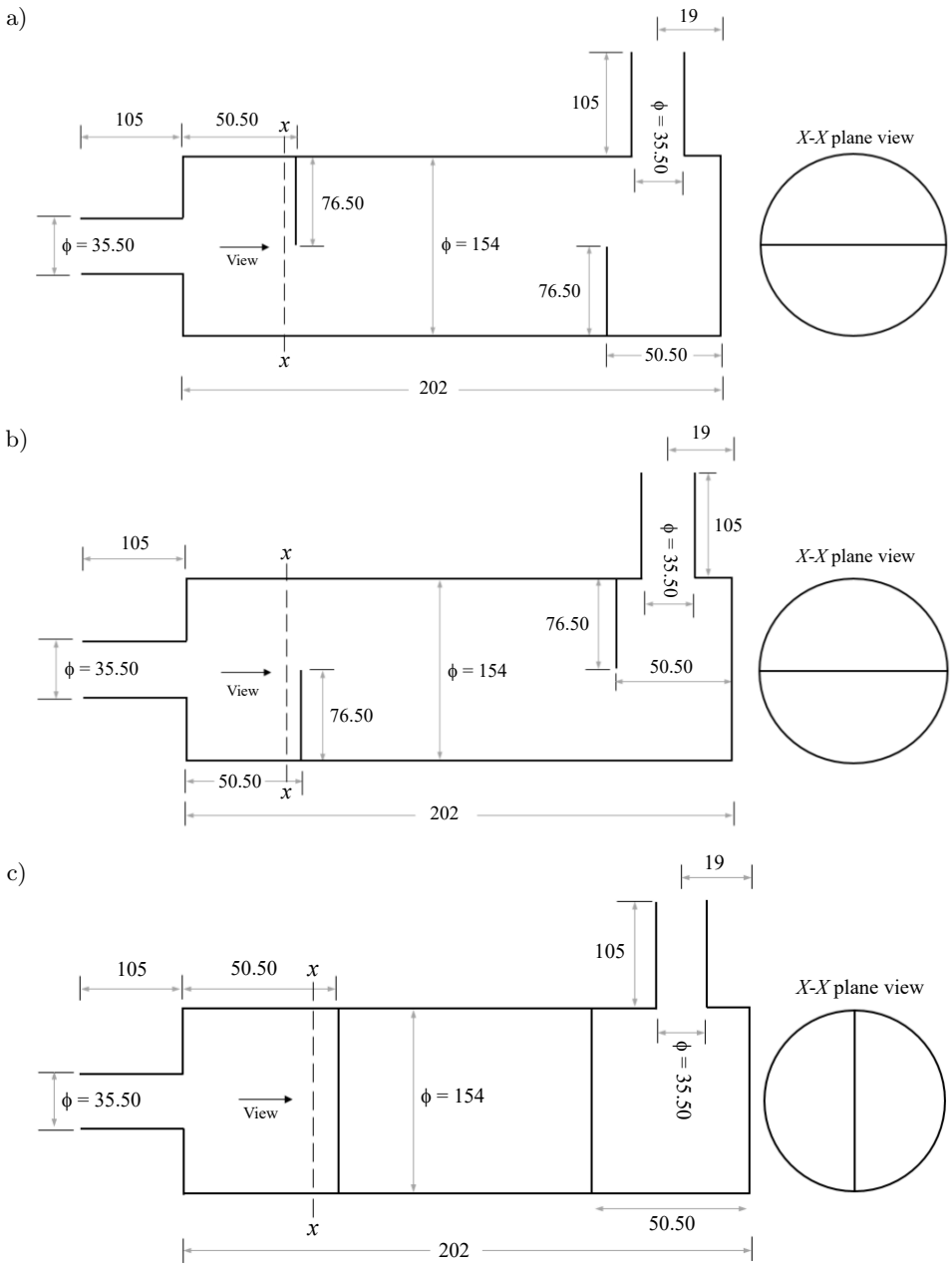

Fig. 2. Computational domains of (a) model_1, (b) model_2, and (c) model_3 of SOMWB (all dimensions are in mm).

putational domains of all the models of SOMWB have been discretized into FLUID 221 elements (10-noded acoustic element). FLUID 221 elements are three-dimensional tetrahedral elements. These elements are useful in modelling the medium for the sound wave propagation. The radiation condition is imposed on the inlet and outlet ports of the SOMWB. The disturbance in the medium is created by applying a surface velocity (equal to 10 m/s) at the inlet. The walls and semi-circular baffles of the SOMWB are set to rigid wall boundary conditions (Vishwakarma, Pawar, 2022). The inlet and outlet ports are defined to calculate the incoming and outgoing rate of sound energy. The calculations of the rate of sound energy at the ports directly determine the TL.

4. Experimental analysis

In this study, a two load method is used for the TL calculation of all models of SOMWB. This method comprises 4 microphones, among which 2 microphones (1 and 2) are positioned along the inlet section and the other 2 microphones (3 and 4) are positioned along the outlet section to determine the progressive and reflective waves. The wave strengths of the decomposed waves are denoted by A, B, C, and D. The wave strengths and the positions of the microphones are shown in Fig. 3. Closed end termination and anechoic termination are the two loads applied in this study for the estimation of TL. Initially, the transfer functions such as $H_{1,\mathrm{ref}}$, $H_{2,\mathrm{ref}}$, $H_{3,\mathrm{ref}}$, and $H_{4,\mathrm{ref}}$ are measured for each load. After evaluation of the transfer functions, 4-pole parameters of the muffler are derived and thereafter the calculation of the TL is done. The 4-pole parameters are derived from the pressure and velocity equations of the wave. As 2 equations are not sufficient for the estimation of 4 pole parameters, 2 different loading conditions are used. For the first load, it is done by closing the outlet using a tube closed at one end, and is shown in Fig. 3a. For the second load, it is closed by using a tube filled with polyester felt (for anechoic termination) and is shown in Fig. 3b.

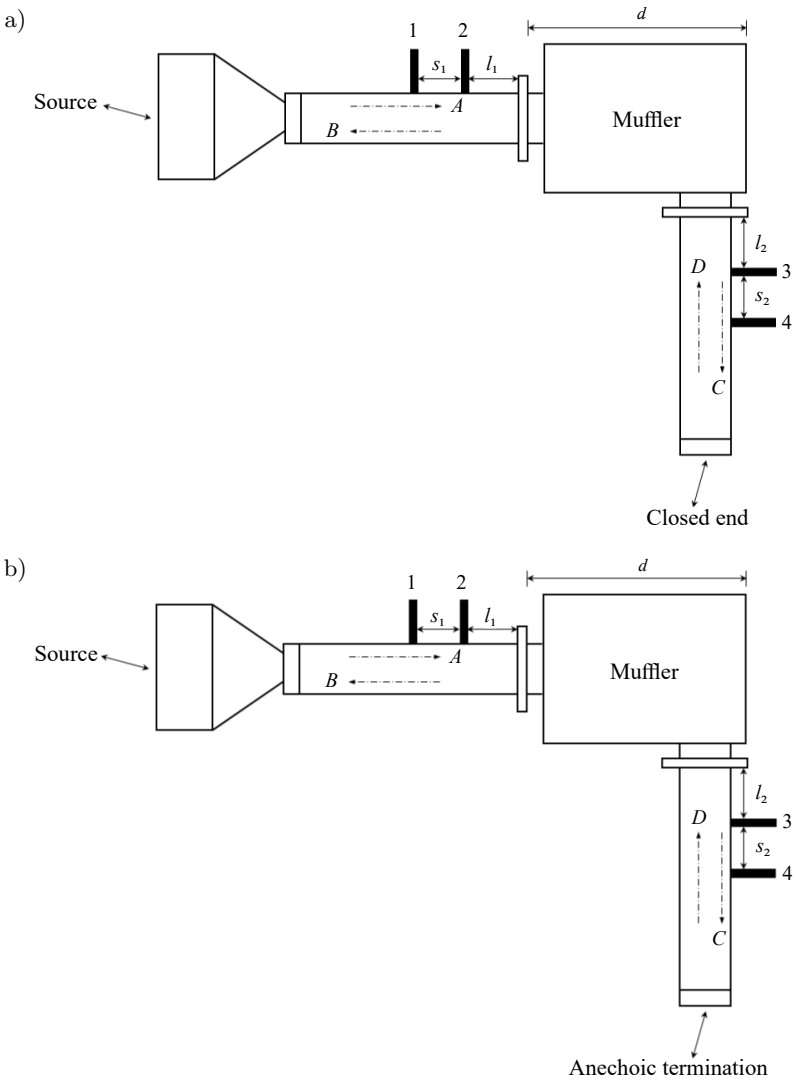

Fig. 3. Two-load setup with (a) closed-end termination and (b) an anechoic termination for estimation of TL of the muffler.

White noise is generated from the speaker and it ranges from 10 Hz to 5000 Hz. After the calibration of the microphones, readings were taken.

Wave decomposition data processing is the most popular method to measure the transfer functions to obtain the sound TL. The pressure relation for one-dimensional moving wave can be given by (Hua, Herrin, 2013):

$$P(x) = A * e^{-jkx} + B * e^{jkx}. \tag{44}$$

The particle velocity for the 1-D moving wave can be given by (Hua, Herrin, 2013):

$$V(x) = (A * e^{-jkx} - B * e^{jkx})/(\rho c). \tag{45}$$

By applying wave decomposition at both the upstream and downstream tubes, the wave strength A, B, C, and D can be determined as

$$A = j\frac{H_{1,\mathrm{ref}}e^{-jkl_1} - H_{2,\mathrm{ref}}e^{-jk(l_1+S_1)}}{2 * \sin(kS_1)}, \tag{46}$$

$$B = j\frac{H_{2,\mathrm{ref}}e^{-j(l_1+S_1)} - H_{1,\mathrm{ref}}e^{-jkl_1}}{2 * \sin(kS_1)}, \tag{47}$$

$$C = j\frac{H_{3,\mathrm{ref}}e^{jk(l_2+S_2)} - H_{4,\mathrm{ref}}e^{jkl_2}}{2 * \sin(kS_2)}, \tag{48}$$

$$D = j\frac{H_{4,\mathrm{ref}}e^{jkl_2} - H_{3,\mathrm{ref}}e^{jk(l_2+S_2)}}{2 * \sin(kS_2)}, \tag{49}$$

where k, x, ρ, and c are wave number, direction of wave propagation, density of medium, and velocity of sound in the medium, respectively.

For different loads, the pressure and particle velocity at two ends of the muffler are expressed as

$$p_0 = A + B, \tag{50}$$

$$u_0 = (A - B)/\rho c, \tag{51}$$

$$p_d = Ce^{-jkd} + De^{jkd}, \tag{52}$$

$$u_d = (Ce^{-jkd} - De^{jkd})/\rho c, \tag{53}$$

where d is the length of the muffler. The transfer matrix based on pressure and particle velocity can be written as

$$\mathbf{T} = \begin{bmatrix} \left[\frac{p_{0a}u_{db} - p_{0b}u_{da}}{p_{da}u_{db} - p_{db}u_{da}}\right] & \left[\frac{p_{0b}p_{da} - p_{0a}p_{db}}{p_{da}u_{db} - p_{db}u_{da}}\right] \\ \left[\frac{u_{0a}u_{db} - u_{0b}u_{da}}{p_{da}u_{db} - p_{db}u_{da}}\right] & \left[\frac{p_{da}u_{0b} - p_{db}u_{oa}}{p_{da}u_{db} - p_{db}u_{da}}\right] \end{bmatrix}, \tag{54}$$

where the subscripts a (anechoic termination) and b (closed end) represent the loads. Then, the TL is expressed as

$$\mathrm{TL} = 20\log_{10}\left|\frac{1}{2}\left(T_{11} + \frac{T_{12}}{\rho c} + \rho c T_{21} + T_{22}\right)\right|. \tag{55}$$

The impedance tube (Alfa Acoustic's tube) is used to evaluate the sound TL in accordance with ASTM E2611 standards. The experimental setup consists of several components such as impedance tubes, microphones, speaker, power amplifier, and a data acquisition system. The impedance tube is circular with an internal and external diameter of 34.90 mm and 40.90 mm. The microphones are pressure field microphones with a diameter of 0.63 mm. A loudspeaker (15 W, 6 Ohm, and 101.6 mm diameter) is used as the source of sound. All measurements are done at ambient conditions. The transfer function method is used in the measurement software. The environmental condition for impedance tube is set with the help of a software. The details of the parameter setup in the impedance tube during the experimentation is given in Table 1. The room temperature, relative humidity, and atmospheric pressure at the time of experimentation were found as 25.7 °C, 55 %, and 101.7 kPa, respectively.

In impedance tube, speed of sound is kept as 347.7 m/s and density of air is 1.183 kg/m^3. Three design models of SOMWB have been fabricated using a 2 mm thick SS 409 and are shown in Fig. 4. The fabricated

Table 1. Impedance tube parameters during experimentation.

Impedance tube parameters	
Frequency range [Hz]	10–5000
Distance between microphones (S_1 and S_2) [mm]	30
Distance between muffler to upstream microphone (l_1) [mm]	90
Distance between muffler to downstream microphone (l_2) [mm]	240
Tube diameter [mm]	45

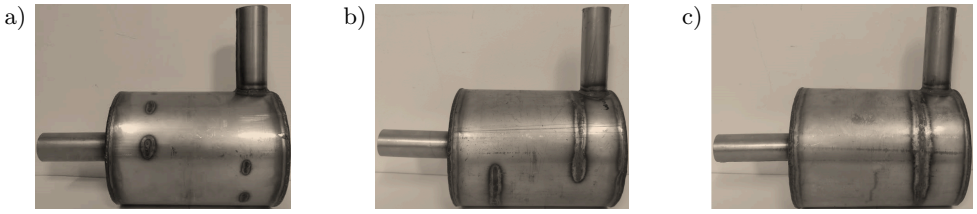

Fig. 4. Fabricated (a) model_1, (b) model_2, and (c) model_3 of the SOMWB.

Fig. 5. Experimental setup for TL measurement of the fabricated mufflers.

muffler is then attached to the impedance tube setup and is shown in Fig. 5, and henceforth, the TL of the muffler is calculated.

5. Results and discussion

5.1. Transmission loss (TL)

The comparison of analytical TL, computational TL, and experimental TL curves for model_1, model_2, and model_3 of SOMWB has been shown in Fig. 6. It can be seen that the orientation of the semi-circular baffles inside the expansion chamber of SOMWB has a serious impact on its TL. The analytical TL curve is the same for the all the models of SOMWB because the analytical modelling does not account for the orientation of the semi-circular baffles as this analysis is one-dimensional. The analytical modelling of the SOMWB is compared with the previously published work (Vishwakarma, Pawar, 2024) on the simple expansion chamber muffler with the side outlet (SECMSO). The comparison indicates that the analytical modelling of SOMWB successfully predicts the presence of semi-circular baffles in the form of increased TL. It also shows that the TL of the SOMWB is greater than TL of SECMSO throughout the entire frequency range except between 1740 Hz–1770 Hz. Analytically, the TL of SOMWB has its maximum value 38.60 dB at 880 Hz. There is an increment of 16 dB in the TL of SOMWB when compared with the SECMSO. From Fig. 6, it can be depicted that the maximum TL's of model_1, model_2, and model_3 obtained from computational modelling are 41 dB (980 Hz), 63.71 dB (2194 Hz), and 75.47 dB (1520 Hz), respectively. The maximum TL of model_1, model_2,

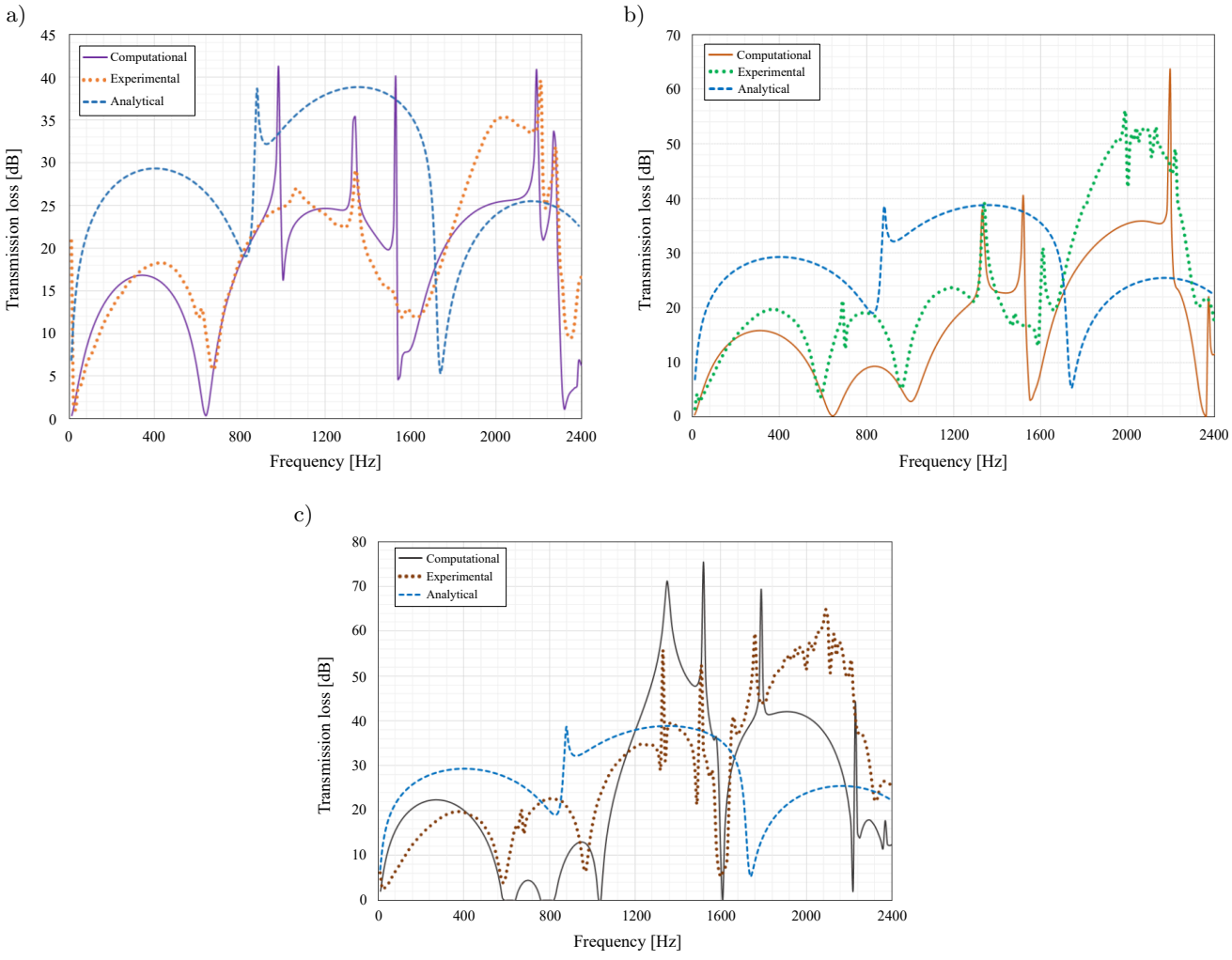

Fig. 6. Comparison of analytical TL, computational TL, and experimental TL for: a) model_1; b) model_2; c) model_3.

and model_3 obtained from experiment are 39.27 dB (2210 Hz), 55.77 dB (1990 Hz), and 64.81 dB (2090 Hz), respectively. This is because of the presence of a multi-chambered expansion chamber in the SOMWB. The semi-circular baffles enhance the effectiveness of the muffler in the mid and high-frequency range (Elsayed *et al.*, 2017). The values of the TL from FEA and experimentation at peaks and troughs for all the models are listed in Tables 2 and 3, respectively. The order of frequencies in a single cell of the table is the frequency for the maximum TL followed by the frequency for the minimum TL. The percentage errors in the comparison of maximum TLs obtained from FEA and experimentation for model_1, model_2, and model_3 are 4.73 %, 12.46 %, and 14.12 %, respectively, and are acceptable. The comparison of the TL curves of SOMWB shows that the analytical modelling of SOMWB is able to capture all the peaks and trough in the TL of SOMWB up to the cut-off frequency. The cut-off frequency (Ih, Lee, 1985; 1987; Åbom, 1990) for all the models of SOMWB comes out to be 1311 Hz. The higher-order modes start to propagate above 1311 Hz. The propagation of the higher-order modes of sound waves can be seen in the FEA and experimental TL curve in the form of abrupt peaks. But the analytical TL curve does not have these peaks because it has the assumption of plane wave propagation only. From Fig. 6a, it can be observed that there are 2 peaks (340 Hz and 980 Hz) and 2 troughs (640 Hz and 1000 Hz) in the computational TL curve before the cut off frequency. The analytical TL curve also shows the 2 peaks (400 Hz and 880 Hz) and 2 troughs (830 Hz and 920 Hz) in the TL with a slight shift in the frequencies for peaks and troughs. The values of TL in the analytical and computational curve are different due to the one- and three-dimensional analysis of the SOMWB, respectively. The experimental values are lower than the FEA values at specific frequencies because the incident sound pressure is completely absorbed by the end outlet in the computational investigation, but the experiment produces reflected sound pressure and other sounds. This is because FEA calculations are based on ideal boundary conditions. Limitations in the accuracy of microphones, manufacturing errors, experimental setup flaws, different environmental conditions, and leakage of sound waves through the connections are the other reasons for the difference in the experimental and FEA values. Although the analytical TL curve and computational TL curve deviate somewhat from the experimental TL curve, the general agreement is good, giving credible information for future investigations identifying the effect mechanism of complicated mufflers. From Table 3 it can be observed that the experimental TL curves for the model_1, model_2, and model_3 have the maximum TL as 39.27 dB, 55.77 dB, and 64.81 dB, respectively. The performance of model_2 is better (42 % higher TL) than model_1 because of the orientation of the second semi-circular baffle. In model_2, the second semi-circular baffle guides the sound wave to travel a longer path as compared to model_1. Similarly, model_3 shows better performance (16.21 % higher TL) than model_2. Therefore, model_3 proves to be the best design for SOMWB in the attenuation of

Table 2. TL values from FEA for all the models at different frequencies.

TL/Frequencies		340/640 [Hz]	980/1000 [Hz]	1340/1490 [Hz]	1530/1540 [Hz]	2190/2220 [Hz]	2270/2320 [Hz]
model_1	Max. TL [dB]	16.81	41.22	35.31	39.76	40.88	33.61
	Min. TL [dB]	0.40	16.45	19.80	4.63	20.96	1.19
TL/Frequencies		310/640 [Hz]	1330/1440 [Hz]	1520/1550 [Hz]	2060/2140 [Hz]	2194/2360 [Hz]	2370/2400 [Hz]
model_2	Max. TL [dB]	15.84	37.75	40.37	35.88	63.71	21.74
	Min. TL [dB]	0.28	22.70	3.14	35.40	0.17	11.57
TL/Frequencies		270/590 [Hz]	950/1030 [Hz]	1350/1470 [Hz]	1520/1570 [Hz]	1790/1830 [Hz]	1910/2220 [Hz]
model_3	Max. TL [dB]	22.41	13.03	71.22	75.47	69.41	42.08
	Min. TL [dB]	0	0	47.98	35.70	41.42	2.80

Table 3. TL values of all the fabricated models from the experiment at different frequencies.

TL/Frequencies		430/670 [Hz]	1070/1290 [Hz]	1340/1560 [Hz]	2040/2160 [Hz]	2210/2230 [Hz]	2280/2350 [Hz]
model_1	Max. TL [dB]	18.24	26.92	29.05	35.32	39.27	31.66
	Min. TL [dB]	5.78	22.32	11.86	33.49	24.70	9.39
TL/Frequencies		370/590 [Hz]	690/700 [Hz]	1340/1590 [Hz]	1610/1660 [Hz]	1990/2000 [Hz]	2360/2400 [Hz]
model_2	Max. TL [dB]	19.67	21.19	39.31	30.92	55.77	21.80
	Min. TL [dB]	3.70	12.50	13.05	19.44	42.10	16.91
TL/Frequencies		370/590 [Hz]	810/970 [Hz]	1330/1320 [Hz]	1510/1490 [Hz]	1760/1600 [Hz]	2090/2330 [Hz]
model_3	Max. TL [dB]	19.79	22.64	45.73	52.30	59.46	64.81
	Min. TL [dB]	4.07	7.35	29.28	21.58	5.29	22.43

sound waves in the 10 Hz–2400 Hz range. For model_1, the first, second, third, fourth, fifth, and sixth peaks in the experimental TL curve occur at 430 Hz, 1070 Hz, 1340 Hz, 2040 Hz, 2210 Hz, and 2280 Hz, respectively. The TL values at the respective peaks are 18.24 dB, 26.92 dB, 29.05 dB, 35.32 dB, 39.27 dB, and 31.66 dB. For the model_2, the first, second, third, fourth, fifth, and sixth peaks in the experimental TL curve occur at 370 Hz, 690 Hz, 1340 Hz, 1610 Hz, 1990 Hz, and 2360 Hz, respectively. The TL values at the respective peaks are 19.67 dB, 21.19 dB, 39.31 dB, 30.92 dB, 55.77 dB, and 21.80 dB. Similarly, the experimental TL curve for the model_3 has the first, second, third, fourth, fifth, and sixth peaks at 370 Hz, 810 Hz, 1330 Hz, 1510 Hz, 1760 Hz, and 2090 Hz, respectively. Experimental TL curves for all models indicate the effectiveness of the models in specific frequency ranges.

5.2. Band power

In the experimental setup, the band power of the sound wave detected by the microphones in the 1/3 octave band is shown in Fig. 7. Band power in the 1/3 octave bands helps in understanding the frequency distribution of noise. Mufflers are designed to attenuate specific frequencies of noise coming from internal combustion engines, so analyzing band power in specific frequency bands provides the effectiveness of mufflers in the suppression of noise across different frequency ranges. Microphone 1 and microphone 3 are chosen for capturing the band power of the progressive sound wave. The magnitude of the band power of the progressive wave detected by microphone 3 is having low value as compared to the microphone 1 for all the models. This is due to the attenuation provided by the muffler. There are fluctuations in the band power at the start. This is due to the weak signal from the loudspeaker at low frequencies, instability and insensitivity of the microphones in capturing the sound wave at the initial stage. After the stability of the microphones, values given by them are within an acceptable range. The difference between the band powers detected by microphone 1 and microphone 3 shows the performance of all models of the SOMWB. The difference is maximum for model_3 of the SOMWB at 2000 Hz (octave middle frequency). The upper and lower frequencies for this band are 1782 Hz and 2245 Hz, respectively. This indicates that the design of the model_3 is suitable for the suppression of the noise in this frequency band. Band power curves for model_3 furthermore suggest other octave middle frequencies, such as 1000 Hz and 1600 Hz where model_3 is effective. In Fig. 6c, the experimental TL curve of the model_3 of SOMWB also indicates that model_3 is highly effective in 1030 Hz–1480 Hz (1000 Hz 1/3 octave band), 1500 Hz–1570 Hz (1600 Hz 1/3 octave band), and 1760 Hz–2400 Hz (1600 Hz 1/3 octave band). The band power curves show that the difference between the band powers detected by microphone 1 and microphone 3 for model_2 of SOMWB is maximum at 1250 Hz and 2000 Hz (octave middle frequencies). Thus, it can be concluded from Fig. 6b and Fig. 7 that model_2 of SOMWB is effective in 1110 Hz–1260 Hz, 1310 Hz–1400 Hz, and 1690 Hz–2300 Hz. Similarly, from Fig. 6a and Fig. 7, it is concluded that model_1 of SOMWB is effective in 880 Hz–1360 Hz and 1800 Hz–2290 Hz.

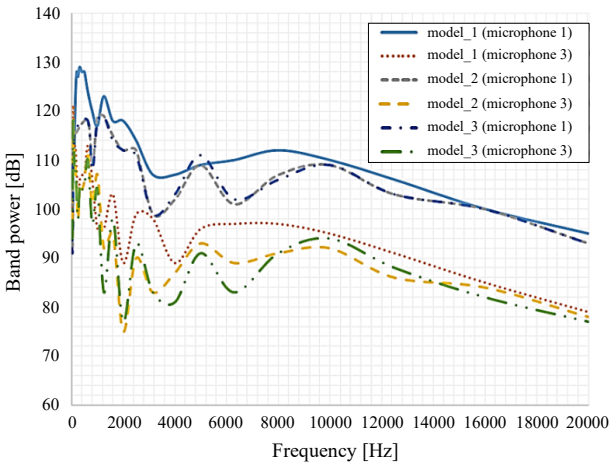

Fig. 7. Comparison of the band powers for model_1, model_2, and model_3 of SOMWB.

5.3. Sound pressure level (SPL)

The SPLs can be presented in isolines form and contour form. The SPL isoline form provides information about the movement of the sound wave inside the SOMWB, whereas the contour form gives the intensity of the SPL inside the SOMWB. The SPL contours are presented for model_3 of the SOMWB at different frequencies and are shown in Fig. 8. The SPLs are presented at 270 Hz, 950 Hz, 1350 Hz, 1520 Hz, 1790 Hz, and 1910 Hz. Among the mentioned frequencies, 270 Hz and 950 Hz are below the cut-off frequency (1311 Hz) of the model_3 of SOMWB. Therefore, there is plain wave propagation of the sound wave, and can be seen in Figs. 8a and 8b. Other mentioned frequencies are above the cut-off frequency, hence higher order modes of sound wave start to propagate and the wave propagation inside the model_3 becomes non-planar. The SPL contours in Figs. 8c–f clearly show the non-planar movement of the sound wave. From Figs. 8a–f, it could be seen that the minimum SPL value is found at 1520 Hz. The SPL contour at 1520 Hz is shown in Fig. 8d. The maximum and minimum SPL at 1520 Hz are 163.52 dB and 53.69 dB respectively, which shows the effectiveness of model_3 of SOMWB. Therefore, at this frequency, noise reduction by the model_3 is maximum and is also supported by the computational TL curve data.

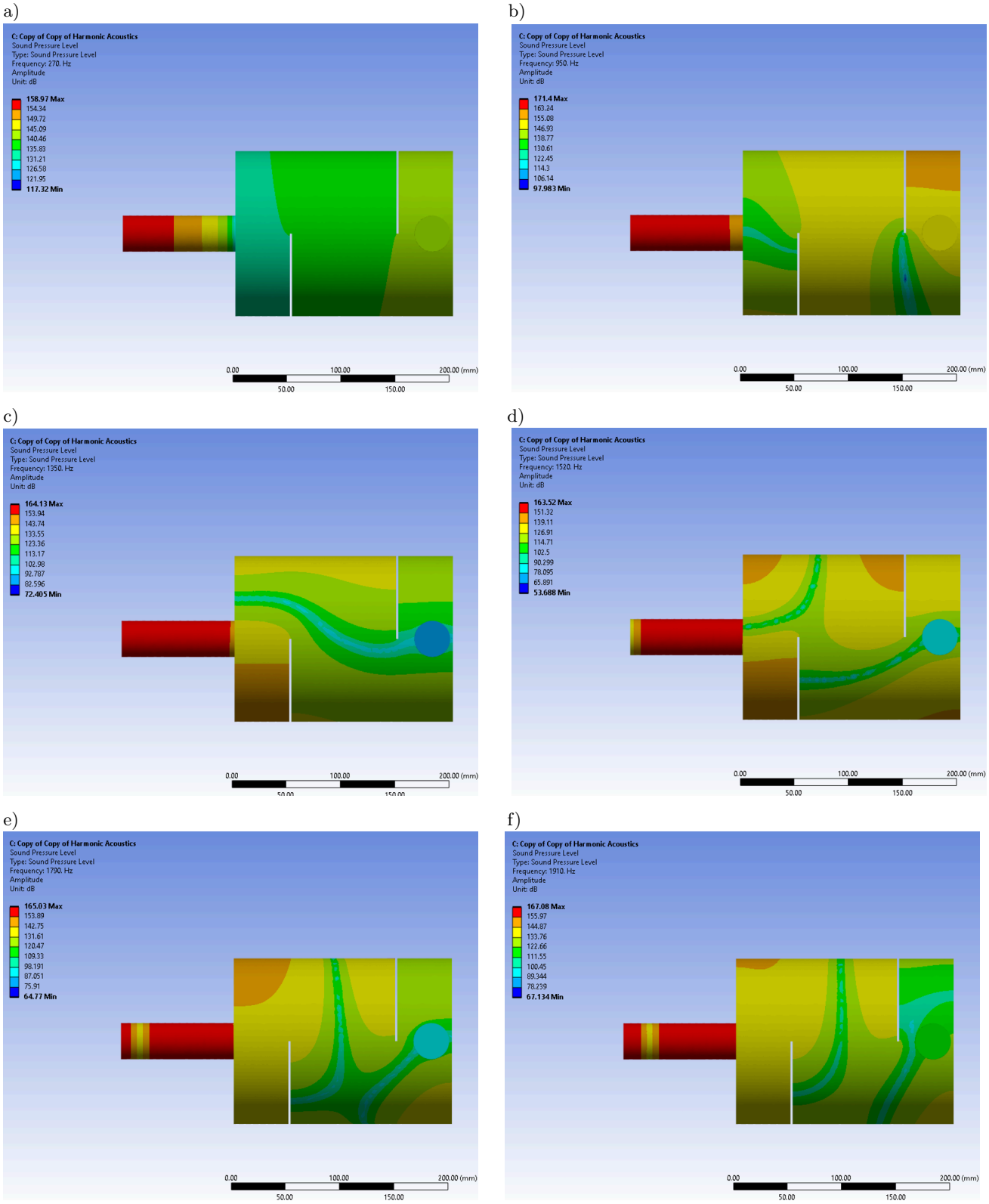

Fig. 8. SPLs at: a) 270 Hz; b) 950 Hz; c) 1350 Hz; d) 1520 Hz; e) 1790 Hz; f) 1910 Hz.

6. Conclusions

The analytical, computational, and experimental acoustical investigations of three models of SOMWB have been successfully done in this study. The analytical modelling of SOMWB is compared with previously published work on SECMSO and it is found that analytical modelling effectively predicts the presence of

semi-circular baffles inside the expansion chamber in the form of increased TL of SOMWB. It is found that there is an increment of 16 dB in the TL of SOMWB as compared to the TL of side outlet muffler without baffles. The computational and experimental TL curves for all the models of SOMWB are in fair agreement. The model_1, model_2, and model_3 of SOMWB show their maximum TL values at different frequencies in the range 10 Hz–2400 Hz. The comparison among the experimental TL curves of all the models concludes that model_2 gives 16.5 dB (42 %) higher TL than model_1. Whereas, model_3 shows 9.04 dB (16.20 %) higher TL than model_2. Through the band power analysis in the 1/3 octave band for all the models of SOMWB it is concluded that model_1 is effective in the range 880 Hz–1360 Hz and 1800 Hz–2290 Hz, model_2 is effective in the range 1110 Hz–1260 Hz, 1310 Hz–1400 Hz, and 1690 Hz–2300 Hz. Model_3 proves to be the best design of SOMWB and is effective for 1030 Hz–1480 Hz, 1500 Hz–1570 Hz, and 1640 Hz–2400 Hz frequency sound waves. The SPL contours of model_3 provides the information about the acoustic wave strength inside the SOMWB at different frequencies. The acoustic wave strength inside the model_3 is minimum at 1520 Hz and this indicates that model_3 can effectively suppress the sound wave of this frequency. The SPL also shows the excitation of higher order modes above the cut-off frequency in the form of non-planar movement of sound waves. This study indicates that the orientations of semi-circular baffles and the outlet on the SEC muffler have a significant impact on its performance. This study is beneficial in the design of the muffler with semi-circular baffles as the internal configuration.

Funding

The authors received no financial support for the research, authorship, and/or publication of this article.

Conflict of interest

The authors declare that they have no known competing financial interests or personal relationships that could have appeared to influence the work reported in this paper.

Data availability

The data that support the findings of this study are available from the corresponding author upon reasonable request.

Author contribution

First author conceptualized the study, done the analysis, and wrote the original draft. Second author performed the evaluation and contributed to data interpretation. All authors reviewed the results and approved the final version of the manuscript.

References

1. Åbom M. (1990), Derivation of four pole parameters including higher order mode effects for expansion chamber mufflers with extended inlet and outlet, *Journal of Sound and Vibration*, **137**(3): 403–418, https://doi.org/10.1016/0022-460X(90)90807-C.
2. ANSYS (2022), Mechanical APDL: 2022R1, Acoustics – Acoustic Fundamental, Chapter 8, Ansys workbench help documentation.
3. Chang Y.-C., Chiu M.-C. (2014), Optimization of rectangular multi-chamber plenums equipped with multiple extended tubes using the BEM, neural networks, and the genetic algorithm, *Journal of Mechanics*, **30**(6): 571–584, https://doi.org/10.1017/jmech.2014.66.
4. Cheng C.Y.R., Wu T.W. (1999), Exhaust muffler design and analysis using a boundary element method based computer program, SAE Technical Paper 1999-01-1661, https://doi.org/10.4271/1999-01-1661.
5. Das S. *et al.* (2022), A novel design for muffler chambers by incorporating baffle plate, *Applied Acoustics*, **197**: 108888, https://doi.org/10.1016/j.apacoust.2022.108888.
6. Davis D.D., Stokes G.M., Moore D., Stevens G.L. (1954), Theoretical and experimental investigation of mufflers with comments on engine-exhaust muffler design, *National Advisory Committee for Aeronautics*, Report 1192, https://ntrs.nasa.gov/api/citations/19930092208/downloads/19930092208.pdf.
7. Done V. *et al.* (2014), Muffler design for a refrigerator compressor, *International Compressor Engineering Conference*.
8. Elsayed A., Bastien C., Jones S., Christensen J., Medina H., Kassem H. (2017), Investigation of baffle configuration effect on the performance of exhaust mufflers, *Case Studies in Thermal Engineering*, **10**: 86–94, http://doi.org/10.1016/j.csite.2017.03.006.
9. Fairbrother R., Varhos E. (2007), Acoustic simulation of an automotive muffler with perforated baffles and pipes, SAE Technical Paper 2007-01-2206, https://doi.org/10.4271/2007-01-2206.
10. Fan W., Guo L.X. (2016), An investigation of acoustic attenuation performance of silencers with mean flow based on three-dimensional numerical simulation, *Shock and Vibration*, **2016**: 6797593, https://doi.org/10.1155/2016/6797593.
11. Gorazd Ł. (2021), Experimental determination of a reflective muffler scattering matrix for single-mode excitation, *Archives of Acoustics*, **46**(4): 667–675, https://doi.org/10.24425/aoa.2021.139643.
12. Gupta A.K. (2016a), Comparison of noise attenuation level by a convergent and divergent cylindrical duct with space constraints, *International Journal of Scientific Research in Science, Engineering and Technology*, **2**(2): 778–781.

13. Gupta A.K. (2016b), Observation for transmission loss by applying multiple baffle plates on single expansion chamber: A simulation approach, *International Journal of Engineering Research and Modern Education*, **1**(1): 2455–4200, http://ijerme.rdmodernresearch.com/wp-content/uploads/2016/04/28.pdf.
14. Gupta A.K., Tiwari A. (2015), Measurement of sound transmission loss on straight and zigzag perforated concentric tube muffler with constant porosity, *International Journal on Emerging Technologies*, **6**(2): 35–40.
15. Horoub M. (2011), Acoustic noise control using multiple expansion chambers, Ph.D. Theisis, King Fahd University of Petroleum and Minerals, Saudi Arabia.
16. Hua X., Herrin D.W. (2013), Practical considerations when using the two-load method to determine the transmission loss of mufflers and silencers, *SAE International Journal of Passenger Cars – Mechanical Systems*, **6**(2): 1094–1101, http://doi.org/10.4271/2013-01-1881.
17. Igarashi J. (1958), *Fundamentals of Acoustical Silencers (I): Theory and Experiment of Low Pass Filters*, Aeronautical Research Institute, University of Tokyo. Aeronautical Research Institute.
18. Ih J.G., Lee B.H. (1985), Analysis of higher order mode effects in circular expansion chamber with mean flow, *The Journal of the Acoustical Society of America*, **77**(4): 1377–1388, https://doi.org/10.1121/1.392029.
19. Ih J.-G., Lee B.-H. (1987), Theoretical prediction of the transmission loss for the circular reversing chamber mufflers, *Journal of Sound and Vibration*, **112**(2): 261–272, https://doi.org/10.1016/S0022-460X(87)80194-3.
20. Ih J.-G. (1992), The reactive attenuation of rectangular plenum chamber, *Journal of Sound and Vibration*, **157**(1): 93–122, https://doi.org/10.1016/0022-460X(92)90569-J.
21. Jayaraman K., Yam K. (1981), Decoupling approach to modeling perforated tube muffler components, *The Journal of the Acoustical Society of America,* **69**(2): 390–396, https://doi.org/10.1121/1.385465.
22. Jeong U.-C., Kim J.-S., Kim Y.-D., Oh J.-E. (2015), Noise reduction of the automobile multi-mode muffler using differential gap control and neural network control, [in:] *Proceedings of the Institution of Mechanical Engineers, Part D: Journal of Automobile Engineering*, **230**(7): 928–941, https://doi.org/10.1177/0954407015597080.
23. Kulkarni M.V., Ingle R.B. (2018), Finite element analysis of double expansion chamber reactive muffler with side outlet, *International Journal of Research and Analytical Reviews,* **5**(4): 758–764.
24. Le Roy T.W. (2011), Muffler characterization with the implementation of the finite element method and experimental techniques, MSc. Thesis, Michigan Technological University, https://doi.org/10.37099/mtu.dc.etds/381.
25. Lee J.K., Oh K.S., Lee J.W. (2019), Methods for evaluating in-duct noise attenuation performance in a muffler design problem, *Journal of Sound and Vibration*, **464**: 114982, https://doi.org/10.1016/j.jsv.2019.114982.
26. Mimani A., Munjal M.L. (2011), Transverse plane wave analysis of short elliptical chamber mufflers: An analytical approach, *Journal of sound and vibration*, **330**(7): 1472–1489, https://doi.org/10.1016/j.jsv.2010.09.035.
27. Mimani A., Munjal M.L. (2012), Acoustical behavior of single inlet and multiple outlet elliptical cylindrical chamber muffler, *Noise Control Engineering Journal*, **60**(5): 605–626, https://doi.org/10.3397/1.3701036.
28. Mundhe V., Deore E. (2015), Design and optimization of perforated muffler in an automobile exhaust system, *International Journal of Applied Research*, **1**(8): 390–395.
29. Munjal M.L. (1975), Velocity ratio-cum-transfer matrix method for the evaluation of a muffler with mean flow, *Journal of Sound and Vibration*, **39**(1): 105–119, https://doi.org/10.1016/S0022-460X(75)80211-2.
30. Munjal M.L. (1987), A simple numerical method for three-dimensional analysis of simple expansion chamber mufflers of rectangular as well as circular cross-section with a stationary medium, *Journal of Sound and Vibration*, **116**(1): 71–88, https://doi.org/10.1016/S0022-460X(87)81321-4.
31. Munjal M.L. (1997), Plane wave analysis of side inlet/outlet chamber mufflers with mean flow, *Applied Acoustics*, **52**(2): 165–175, https://doi.org/10.1016/S0003-682X(96)00053-9.
32. Mohamad B., Karoly J., Zelentsov A., Amroune S. (2021), Investigation of perforated tube configuration effect on the performance of exhaust mufflers with mean flow based on three-dimensional analysis, *Archives of Acoustics*, **46**(3): 561–566, https://doi.org/10.24425/aoa.2021.138148.
33. Narayana T.S.S., Munjal M.L. (2005), Prediction and measurement of the four-pole parameters of a muffler including higher order mode effects, *Noise Control Engineering Journal*, **53**(6): 240–246, https://doi.org/10.3397/1.2839259.
34. Reddy K.P.K., Fatima S., Mohanty A.R. (2017), A new sound quality metric for the design of engine exhaust mufflers, *Proceedings of the Institution of Mechanical Engineers, Part D: Journal of Automobile Engineering*, **232**(2): 254–263, https://doi.org/10.1177/0954407017696608.
35. Seybert A.F., Cheng C.Y.R. (1987), Application of the boundary element method to acoustic cavity response and muffler analysis, *Journal of Vibration, Acoustics, Stress, and Reliability in Design*, **109**(1): 15–21, https://doi.org/10.1115/1.3269388.
36. Siano D., Auriemma F., Bozza F. (2010), Pros and cons of using different numerical techniques for transmission loss evaluation of a small engine muffler, SAE Technical Paper 2010-32-0028, https://doi.org/10.4271/2010-32-0028.

37. Sullivan J.W. (1979), A method of modeling perforated tube muffler components. I. Theory, *The Journal of the Acoustical Society of America*, **66**(3): 772–778, https://doi.org/10.1121/1.383679.

38. Sullivan J.W., Crocker M.J. (1978), Analysis of concentric tube resonators having unpartitioned cavities, *The Journal of the Acoustical Society of America*, **64**(1): 207–215, https://doi.org/10.1121/1.381963.

39. Tao Z., Seybert A.F. (2003), A review of current techniques for measuring muffler transmission loss, SAE Technical Paper 2003-01-1653, https://doi.org/10.4271/2003-01-1653.

40. Vishwakarma S.K., Pawar S.J. (2021), Simulation studies on the transition from simple expansion chamber muffler to tapered expansion chamber muffler, [in:] *Advances in Fluid and Thermal Engineering. Lecture Notes in Mechanical Engineering*, pp. 389–398, https://doi.org/10.1007/978-981-16-0159-0_34.

41. Vishwakarma S.K., Pawar S.J. (2022), Analytical and computational acoustic modeling of side outlet muffler and its extension in the modeling of tapered side outlet muffler, *Archives of Acoustics*, **47**(4): 491–499, https://doi.org/10.24425/aoa.2022.142893.

42. Vishwakarma S.K., Pawar S.J. (2024), Analytical, computational, and experimental investigations on the impact of side outlet on the simple expansion chamber with axial outlet, *Noise & Vibration Worldwide*, **55**(9–10): 473–480, https://doi.org/10.1177/09574565241278721.

43. Wang C.-N. (1999), A numerical analysis for perforated muffler components with mean flow, *Journal of Vibration and Acoustics*, **121**(2): 231–236, https://doi.org/10.1115/1.2893969.

44. Xiang L., Zuo S., Wu X., Zhang J., Liu J. (2016), Acoustic behaviour analysis and optimal design of a multi-chamber reactive muffler, *Proceedings of the Institution of Mechanical Engineers, Part D: Journal of Automobile Engineering*, **230**(13): 1862–1870, https://doi.org/10.1177/0954407016630112.

45. Yi S.-I., Lee B.-H. (1986), Three-dimensional acoustic analysis of circular expansion chambers with a side inlet and a side outlet, *The Journal of the Acoustical Society of America*, **79**(5): 1299–1306, https://doi.org/10.1121/1.393709.

46. Yu X., Tong Y., Pan J., Sun H., Cheng L. (2016), On the retrofitted design of a truck muffler with cascaded sub-chambers, *Noise Control Engineering Journal*, **64**(5): 602–607, https://doi.org/10.3397/1/376404.

47. Zhao B., Li H. (2022), Analysis of the influencing factors of the acoustic performance of the muffler considering acoustic-structural coupling, *Archives of Acoustics*, **47**(4): 479–490, https://doi.org/10.24425/aoa.2022.142900.

48. Zheng S., Kang Z., Lian X. (2012), Acoustic simulation for exhaust silencer of vehicle engine with combined one/three-dimensional approach, *International Journal of Vehicle Design*, **60**(1/2): 57–70, http://doi.org/10.1504/IJVD.2012.049164.